Journal of Power Sources 650 (2025) 237480

Contents lists available at ScienceDirect

Journal of Power Sources

journal homepage: www.elsevier.com/locate/jpowsour

Enhanced hydrogen generation through electrodeposited non-precious metal Zn/Cu-BTC metal-organic frameworks on indium tin oxide

Carmen Castro-Castillo [a,*], Rodrigo Espinoza-González [a], Pedro P. Jofré-Ulloa [b,c], Maximina Luis-Sunga [d], Nataly Silva [e], Jonathan Suazo-Hernández [f,g], Mónica Soler [a], Mauricio Isaacs [b,c], Gonzalo García [d,**]

[a] Department of Chemical Engineering, Biotechnology and Materials, FCFM, Universidad de Chile, Avenida Beauchef 850, Santiago, Chile
[b] Facultad de Química, Pontificia Universidad Católica de Chile, Vicuña Mackenna 4860, Macul, 7820436, Santiago, Chile
[c] Millennium Institute on Green Ammonia as Energy Vector-MIGA, Pontificia Universidad Católica de Chile, 7820436, Santiago, Chile
[d] Instituto Universitario de Materiales y Nanotecnología, Departamento de Química, Universidad de La Laguna, P.O. Box 456, Santa Cruz de Tenerife, Spain
[e] Facultad de Diseño, Universidad del Desarrollo, Avenida Plaza 680, 7610658, Las Condes, Santiago, Chile
[f] Center of Plant, Soil Interaction and Natural Resources Biotechnology, Scientific and Biotechnological Bioresource Nucleus (BIOREN-UFRO), Universidad de La Frontera, Avenida Francisco Salazar, 01145, Temuco, Chile
[g] Facultad de Medicina Veterinaria y Agronomía, Universidad de Las Américas, Sede Concepción, Chile

HIGHLIGHTS

- Low-cost non-precious metal catalysts for hydrogen production were developed.
- Cu and Zn in conjunction with BTC and without a binder were electrodeposited on ITO.
- Crystalline BTC-based MOF catalysts were created with uniform deposition on ITO.
- Zn/Cu-BTC/ITO electrocatalyst exhibits high catalytic performance toward the HER.

GRAPHICAL ABSTRACT

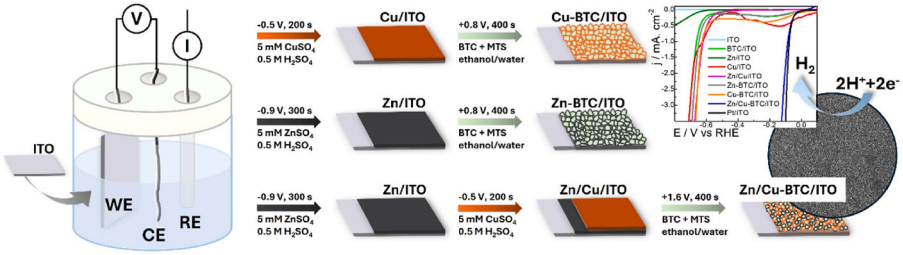

ARTICLE INFO

Keywords:
ITO
MOF
Electrocatalysts
Electrocatalysis
Electrodeposition
HER
Electrolyzer

ABSTRACT

The production of high-purity hydrogen for primary energy generation is a key goal in the renewable energy consumption model. Currently, hydrogen production through electrolysis remains quite expensive, making the development of new non-noble metal catalysts for the cathodes of acidic electrolyzers a promising strategy to lower the costs associated with this technology. In this work, Cu, Zn and Zn/Cu particles in the absence and the presence of 1,3,5-benzenetricarboxylic acid (BTC) have been synthesized via binder-free electrodeposition onto an indium tin oxide (ITO) surface as electrocatalysts to improve the hydrogen evolution reaction (HER) in acidic media. Main results highlight the fundamental role of the metal-organic framework (i.e., BTC), combined with the synergistic effect of both metal elements (i.e., Zn and Cu), in creating a uniform deposition of small crystalline particles on the ITO surface. Consequently, a low-cost and robust electrocatalyst (Zn/Cu-BTC/ITO) with enhanced catalytic performance toward the HER was synthesized. Finally, this work emphasizes how electrochemically modified surfaces, created using low-cost metals and straightforward sustainable synthesis methods,

* Corresponding author.
** Corresponding author.
E-mail addresses: carmen.castro.c@uchile.cl (C. Castro-Castillo), ggarcia@ull.edu.es (G. García).

https://doi.org/10.1016/j.jpowsour.2025.237480
Received 9 February 2025; Received in revised form 20 May 2025; Accepted 23 May 2025
Available online 31 May 2025

can generate atomically dispersed active sites that enhance both electrocatalytic activity and stability. This approach could contribute to the development of innovative electrodes, improving performance while reducing the cost of electrolyzers.

1. Introduction

The increasing global energy consumption, driven by population growth and industrialization, has relied heavily on fossil fuels, which release pollutants—such as CO_2, CO, sulfur oxides, nitrogen oxides and unburned hydrocarbons—contributing to climate change [1–3]. Since these fuels are non-renewable, alternative energy sources will be essential once reserves are depleted [4]. In this context, the hydrogen (H_2) economy is emerging as a promising solution. The hydrogen evolution reaction (HER) is gaining attention for its potential in eco-friendly energy storage and conversion, particularly in fuel cells [4–6]. Water splitting is considered one of the most efficient methods to produce hydrogen, requiring only water and generating H_2 and oxygen (O_2) with minimal environmental impact. In a typical water electrolysis system, O_2 is generated at the anode through the oxygen evolution reaction (OER), while H_2 is produced at the cathode via the HER [7], as shown in reactions 1 and 2:

$$4H^+ + 4e^- \leftrightarrow 2H_2 \quad E^0 = 0.0 \text{ vs RHE} \tag{1}$$

$$2H_2O \leftrightarrow 2O_2 + 4H^+ + 4e^- \quad E^0 = 1.23 \text{ vs RHE} \tag{2}$$

Electrolysis in acidic media is advantageous due to the availability of protons (H^+) for the reduction reaction at the cathode. However, it faces kinetic challenges, such as low exchange current density, which requires high overpotentials and additional energy for efficient operation [8,9]. To overcome these challenges, a suitable electrocatalyst is essential. In an acidic medium, protons are reduced at the cathode to generate $H_{2(g)}$, making the optimization of this reaction crucial for improving electrolyzer efficiency. The acidic environment not only supports the reaction but also enhances overall electrolysis performance [10]. Developing advanced electrocatalysts requires identifying active sites and understanding the relationship between their structures and performance. Commonly studied electrocatalysts include noble metals (e.g., ruthenium (Ru), iridium (Ir), and platinum (Pt)), as well as transition metals [11]. Pt-based electrodes are the most active for HER, but their high cost and limited availability hinder widespread use [12,13]. As a result, significant efforts have been made to identify more affordable and abundant alternatives, with several promising candidates demonstrating comparable efficiency [14–16].

Zinc (Zn), with a standard reduction potential of −0.76 V, is considered a promising material for the HER due to its ability to donate electrons and reduce H^+ to $H_{2(g)}$. However, despite this theoretical reactivity, Zn/ITO electrodes show limited catalytic activity in the HER, attributed to the absence of a proper reduction environment that prevents the recovery of metal ions to their metallic form [17]. Zinc is abundant, safe, easy to handle and economical, making it attractive for industrial and experimental applications. In acidic media, zinc reacts with acids to release hydrogen in a controlled manner, contributing to the safety of the process. In comparison, copper (Cu) offers better corrosion resistance but is less effective in reducing H^+ under acidic conditions, making it less efficient for the HER [18]. The combination of Zn and Cu metals has been proposed as a promising alternative to create a significant potential difference, improving the HER efficiency. Copper's corrosion resistance enhances system durability, while Zinc's reactivity aids in hydrogen production [19]. The synergy between these metals can improve both efficiency and stability, making them suitable for various applications [20]. Moreover, both metals are stable in acidic environments, although their behavior can vary depending on acid concentration and temperature. In acidic solutions, Cu tends to form complexes and may not dissolve easily, while Zn dissolves more readily, releasing hydrogen and forming Zn salts [21].

In recent years, various studies have explored the development of new electrocatalysts, particularly those combining transition metals with non-metals such as carbon (C), nitrogen (N), sulfur (S), oxygen (O), and phosphorus (P) atoms [22,23]. The intrinsic, electronic and structural properties of different compounds have significantly enhanced performance in electrocatalytic applications [24,25]. Among the most promising candidates are metal-organic frameworks (MOFs), which offer atomically dispersed active sites, large surface area, high porosity, controllable morphology and tunability, all of which have attracted considerable attention [26]. MOFs, composed of metal ions and organic ligands, exhibit structural and electronic diversity, making them suitable for applications such as gas adsorption, detection, separation and conversion. The properties of MOFs, including their stability, size and crystal shape can be controlled, which has led to their use in a variety of practical applications, including nanotechnology, electrical devices, catalytic coatings, and other advanced smart technologies. The fabrication of MOF thin films has emerged as an area of interest, focusing on controlling their growth on surfaces to specific porosities [27]. Given these advantages, MOFs have gained significant attention as potential electrocatalysts for water splitting [28–31].

Several studies have explored MOFs as electrocatalysts for electrode deposition or coating, employing techniques such as solvothermal synthesis [32], vapor phase deposition [33], direct growth [34] and electrochemical deposition [35,36]. However, many conventional methods involve challenging conditions such as high temperature and pressure. Electrochemical methods offer a promising solution to overcome these issues. Thin films of electrochemically synthesized MOFs require metal ions, organic ligands, and electrolytes as precursors, and using different metals as electrodes allows for precise control over the structure and surface behavior of MOF thin films, such as crystallinity, morphology, roughness and thickness.

A recent study reported the use of a metal-organic structure derived from Cu/Pt-BTC (BTC: 1,3,5-benzenetricarboxylic acid) as an electrocatalyst [31]. The modified electrode demonstrated excellent catalytic effect for HER, with reduced applied potential and increased current density compared to other test electrodes. However, the use of Pt in the bimetallic MOF increases the material's cost. This approach proposes a new method for manufacturing high-performance electrocatalysts on various substrates using sustainable, high-speed, and easy-to-synthesize processes that minimize toxic waste and can be carried out at a microliter scale, consuming only small amounts of reagents [31].

This study focuses on the development of low-cost, high-performance Zn/Cu-BTC MOFs as electrocatalysts for the HER. The MOFs were synthesized via *in situ* electrosynthesis on an ITO surface (Scheme 1), without the use of binders or functional groups, to evaluate their electrocatalytic efficiency. The stability of the metals in acidic media and their impact on HER performance were investigated. Specifically, it was found that copper, due to its tendency to form complexes, may reduce its own reduction activity, while zinc, which tends to dissolve and release ions, can enhance hydrogen production. The hypothesis proposed is that the synergy between Zn and Cu in the MOF structure may further optimize electrocatalytic efficiency, leading to improved hydrogen evolution.

2. Experimental section

2.1. Chemicals and reagents

Methyltributylmethylammonium sulfate (MTS) was synthesized

from tributylmethylammonium chloride and methyl sulfate, sodium salt hydrate. 1,3,5-benzenetricarboxylic acid (BTC) (98 %), copper sulfate pentahydrate ($CuSO_4{\cdot}5H_2O$, 99 %), zinc sulfate heptahydrate ($ZnSO_4.7H_2O$, 99 %), absolute ethanol (EtOH) and sulfuric acid (H_2SO_4, 95–98 %) were purchased from Sigma-Aldrich, and ultrapure water (Milli-Q Millipore system, 18.2 MΩ cm) was used to prepare all solutions.

2.2. Physicochemical characterization

The surface of the modified electrodes was characterized using several techniques. Field Emission Scanning Electron Microscopy (FE-SEM) coupled with Energy-Dispersive X-ray Spectroscopy (EDX), using a ZEISS GeminiSEM 360 with NanoVP, provided detailed imaging and elemental analysis.

X-ray photoelectron spectroscopy (XPS) analysis was performed using the Surface Analysis Station 1, model XPS RQ300/2, employing aluminum (Al) radiation at an energy of 1486.6 eV. The detector was operated at a voltage of 15 kV and a current of 10.0 mA, with a DESA 150 detector at 2700 V. The scan range spans from 1200 to 0 eV, with a step size of 1 eV or 0.2 eV and a step time of 0.2–0.5 s.

X-ray diffraction (XRD) measurements of the modified electrodes were conducted on a Bruker D8 diffractometer, utilizing CuKα radiation (λ = 1.5418 Å). Data were collected at room temperature with a step size of 0.01° and scan speed of 0.1 s. The X-ray tube operated at 40 kV and 30 mA, and the Rietveld refinement of the XRD patterns was performed using TOPAS Software, employing a pseudo-Voigt function as the profile function.

The modified Scherrer equation as follows was used to determine the crystallite size:

$$D = \frac{k\,\lambda}{\beta \cos\theta} \tag{3}$$

where ***D*** is the size of the crystallite in nm, ***k*** is Scherrer's constant, ***λ*** is the wavelength of the radiation used in diffraction, ***β*** is the full width at half maximum (FWHM) of the peak in radians, and ***θ*** is the diffraction angle in radians.

Attenuated Total Reflectance (ATR) Fourier Transform Infrared (FTIR) spectroscopy was used to analyze the modified electrodes, using a Thermo Scientific Nicolet iS50 FTIR spectrometer equipped with a liquid nitrogen-cooled narrow-band mercury cadmium telluride (MCT) detector. For surface analysis, a variable angle specular reflection accessory (VEEMAX III from PIKE Technologies) with manual and automated angle control was employed.

2.3. Electrochemical characterization

Electrodeposition and electrochemical measurements were performed using an Autolab potentiostat/galvanostat (model PGSTAT204) at ambient temperature and pressure, in a three-electrode electrochemical system. A Pt wire and an Ag/AgCl wire in 3.5 M KCl solution were used as the counter and reference electrodes, respectively, while a modified ITO electrode served as working electrode. Cyclic voltammetry (CV) was conducted in 0.5 M H_2SO_4 solution saturated with Ar (pH 0.38), at a scan rate of 100 mV s^{-1}. The reference potentials can be converted to the RHE scale using the following formula:

$$E_{RHE} = E_{Ag/AgCl} + 0.059\ V\ x\ pH \tag{4}$$

All potentials mentioned in this document are referenced to the RHE scale, unless stated otherwise.

Each CV was normalized based on the geometric area of 0.3 cm^2 to ensure the comparability of the data obtained in the different experiments conducted.

2.3.1. Electrochemically active surface area measurement

The electrochemically active surface area (ECSA) was determined using the double-layer capacitance method, as described in previous studies [31,37]. Cyclic voltammograms were recorded for the modified ITO electrodes at different scan rates, in an Ar-purged 0.5 M H_2SO_4 solution, within a potential range where no faradaic current was observed. At higher scan rates, the oxidation or reduction of non-electrolytic species may become less efficient, potentially affecting the surface area calculation. The value was determined using the following equations [31,38].

$$\Delta I = 2v^{*}Cdl \tag{5}$$

$$ECSA = \frac{Cdl}{Cdl'} \tag{6}$$

where (I) is the current density, (ν) is the scan rate in the CV study, (Cdl) is the double layer capacitance and (Cdl') is the specific capacitance of an atomically smooth material (~20 μF cm^{-2} [38]).

2.3.2. Electrocatalytic hydrogen evolution reaction

To investigate the catalytic performance of the modified ITO electrodes, linear scanning voltammetry (LSV) curves were measured at a scan rate of 5.0 mV s^{-1} in a 0.5 M H_2SO_4 electrolyte (pH = 0.38), which was Ar-purged at room temperature (25 °C).

2.3.3. Electrochemical impedance spectroscopy study (EIS)

The electrochemical impedance study was performed on IVIUM-STAT, IVIUM Technologies. Arbin test station (BT2043) at an amplitude of 1 mV from 0.1 Hz to 10 KHz in a 0.5 M H_2SO_4.

2.3.4. Electrocatalytic stability for HER

Electrocatalytic stability was evaluated through chronopotentiometry during the HER by applying a constant current density of −2 mA/cm^{-2} in 0.5 M H_2SO_4 solution for 12 h at room temperature (25 °C).

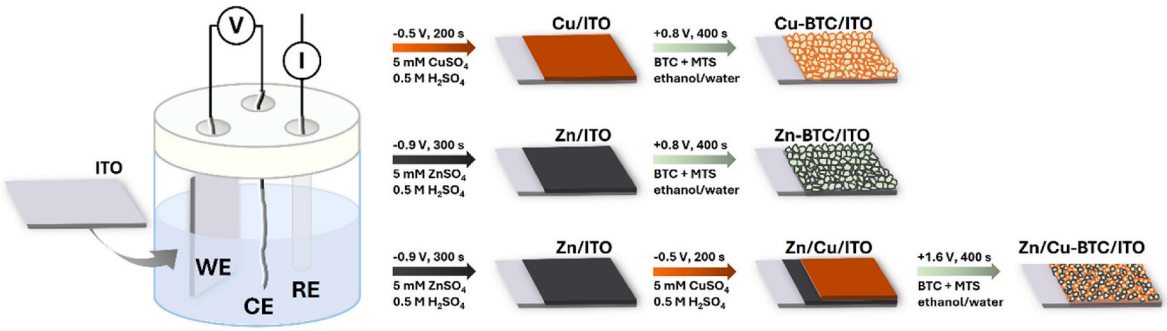

Scheme 1. Principal steps to produce the catalysts employed in the current work.

2.3.5. Quantification of hydrogen by controlled current electrolysis

To perform the electrolysis at controlled current, a type H cell with a Nafion® membrane was used, along with a three-electrode system: a working electrode, a graphite counter electrode, and an Ag/AgCl reference electrode in a 3.5 M KCl solution. The experiment was conducted for 1 h at −2 mA, in 0.5 M H_2SO_4 at room temperature (25 °C).

To quantify the gaseous product, 50 μL samples were extracted from the headspace of the cathode using a gas-tight syringe and injected into a DANI MASTER gas chromatograph (GC) equipped with a micro-volume μTCD detector. A Supelco silica column with molecular sieves (5′) measuring 30 m × 0.53 mm was used. High-purity argon served as the carrier gas.

The GC was calibrated using ultrapure H_2 gas as a standard (INDURA), which contains a certified molar percentage. Calibration was performed three times, with the average peak areas used to ensure repeatability. The concentration of the gaseous product was calculated based on pre-established calibration curves using gas standards.

The Faradaic efficiency (FE) measurements for H_2 were calculated using the following equations:

$$n_{exp} = C_{H_2} x\ V_{gas} \tag{7}$$

$$n_{teo} = \frac{Q_t}{v\ F} \tag{8}$$

$$FE = \frac{n_{exp}}{n_{teo}}\ x\ 100\ \% \tag{9}$$

where C is the concentration of H_2 obtained in mM, V is the volume of the cell in L, Q is the system charge in coulombs C, n represents the moles of H_2 generated (both experimental and theoretical), F is Faraday's constant, and v is the valency of the ions involved in the reaction.

2.4. Electrochemical synthesis of modified electrodes

2.4.1. ITO pretreatment

The cleaning procedure for substrates was performed in a laminar flow hood. Twenty ITO substrates were placed in Teflon blocks and immersed in a 1 % Alconox detergent solution in deionized water. Each substrate was cleaned and rinsed in a DI water bath, followed by sonication. Next, they were treated with acetone, and the process was repeated with isopropanol. Finally, the substrates were dried with argon, checked for residues, and stored in substrate holders, keeping them in a vacuum desiccator.

All electrochemical syntheses were performed at room temperature.

2.4.2. BTC-modified ITO electrochemical synthesis (BTC/ITO)

BTC-modified ITO (BTC/ITO) was fabricated in a solution containing 15 mmol of BTC as a linker and 33 mmol of MTS as an electrolyte in 100 mL of EtOH/H_2O (H_2O: EtOH = 30:70 v/v%). A constant potential of +0.80 V vs. RHE was then applied to the ITO working electrode. As a result, BTC/ITO was formed on the surface of ITO after 400 s, without any binder or functional group pH ≈ 7.0. The synthesis was conducted in a similar way as described by M. Malakzadeh [31].

2.4.3. Cu-modified ITO electrochemical synthesis (Cu/ITO)

Cu-modified ITO (Cu/ITO) was prepared by electrodeposition in a solution of 5 mM $CuSO_4$ and 0.5 M H_2SO_4. A constant potential of −0.50 V vs. RHE was applied for 200 s, leading to the uniform deposition of metallic Cu on the ITO surface, resulting in the formation of Cu/ITO. The pH remained constant at 0.38.

2.4.4. Zn-modified ITO electrochemical synthesis (Zn/ITO)

Zn-modified ITO (Zn/ITO) was synthesized similarly but using a solution of 5 mM $ZnSO_4$ and 0.5 M H_2SO_4. A constant potential of −0.90 V vs. RHE was applied for 300 s, facilitating the uniform deposition of metallic Zn onto the ITO surface, thereby forming Zn/ITO. The applied potential did not alter the concentration of H^+ ions in this situation. This did not change the pH directly, which remained constant at 0.38.

2.4.5. Zn/Cu-modified ITO electrochemical synthesis (Zn/Cu/ITO)

For the electrodeposition of bimetallic Zn/Cu particles on the ITO surface, Zn was first electrodeposited from a 5.0 mM $ZnSO_4$ solution in 0.5 M H_2SO_4 by applying a potential of −0.9 V vs. RHE for 300 s. Subsequently, Cu was deposited from a 5.0 mM $CuSO_4$ solution in 0.5 M H_2SO_4 by applying −0.50 V vs. RHE for 200 s. This two-step process resulted in the formation of Zn/Cu/ITO. The pH remained constant at 0.38.

2.4.6. Cu-BTC- modified ITO electrochemical synthesis (Cu-BTC/ITO)

Cu particles were first electrodeposited on the ITO surface as described in Section 2.4.2. Then, a BTC solution was prepared according to the method outlined in Section 2.4.1 and applied to the Cu/ITO, resulting in the formation of Cu-BTC/ITO.

2.4.7. Zn-BTC- modified ITO electrochemical synthesis (Zn-BTC/ITO)

Zn particles were first electrodeposited on the ITO surface as described in Section 2.4.3. Then, a BTC solution was prepared according to the method outlined in Section 2.4.1, which was applied to the Zn/ITO, resulting in the formation of Zn-BTC/ITO.

2.4.8. Zn/Cu-BTC- modified ITO electrochemical synthesis (Zn/Cu-BTC/ITO)

The procedure outlined in Section 2.4.4 was initially used to deposit Zn and Cu on the ITO surface. Afterward, the Zn/Cu/ITO electrode was immersed in the MOF electrosynthesis solution (as described in Section 2.4.1), and a potential of +1.6 V vs. RHE was applied for 400 s to facilitate the formation of Zn/Cu-BTC/ITO.

2.4.9. Pt- modified ITO electrochemical synthesis (Pt/ITO)

For comparison, Pt was electrodeposited on ITO using a 5 mM K_2PtCl_6 solution in H_2SO_4. A potential of 0.0 V vs. RHE was applied for 200 s, obtaining a Pt/ITO electrode.

3. Results and disscussion

3.1. Structural characteristics

The morphological and structural characterization of the electrodes was carried out using FE-SEM. Fig. 1A and B illustrate the modified surface of the ITO electrode under the application of a stable voltage in acidic solutions with $CuSO_4$ and $ZnSO_4$, respectively. Both figures reveal amorphous surface morphologies; however, the electrodeposition of Zn (Fig. 1B) presents a more uniform metallic coating compared to the electrodeposition of Cu (Fig. 1A). Furthermore, the electrodeposition of both metals Zn/Cu on the ITO surface resulted in complete coverage, with irregular metallic shapes approximately 153 nm in size (Fig. 1C). The study also examined the BTC ligand, where the formation of microporous particles on metal-free ITO was observed. The morphology and size of the BTC/ITO revealed a distinct cubic shape with well-defined edges. Furthermore, material morphology exhibits an irregular surface with cracks and a porous structure [39], as depicted in Fig. 1D, with a size of 793 nm. On the other hand, Fig. 1E showed the particles of Cu-BTC/ITO, which had an irregular octahedral shape, with a particle size of 413 nm. In contrast, Zn-BTC/ITO (Fig. 1F) displays a structure resembling an elongated cubic shape, with a size of 417 nm (considering the narrowest lake). Fig. 1G and H reveal the high uniformity of the Zn/Cu-BTC nanoparticles deposited on ITO. The bimetallic nanoparticles (NPs) assembled in the MOF structure are arranged in octahedral and tetrahedral networks, with a narrow size distribution of approximately 54 nm. These nanoparticles were the smallest of all the prepared catalysts, leading to an increase in surface area. Fig. S1 shows the particle size distribution of materials synthesized in the current

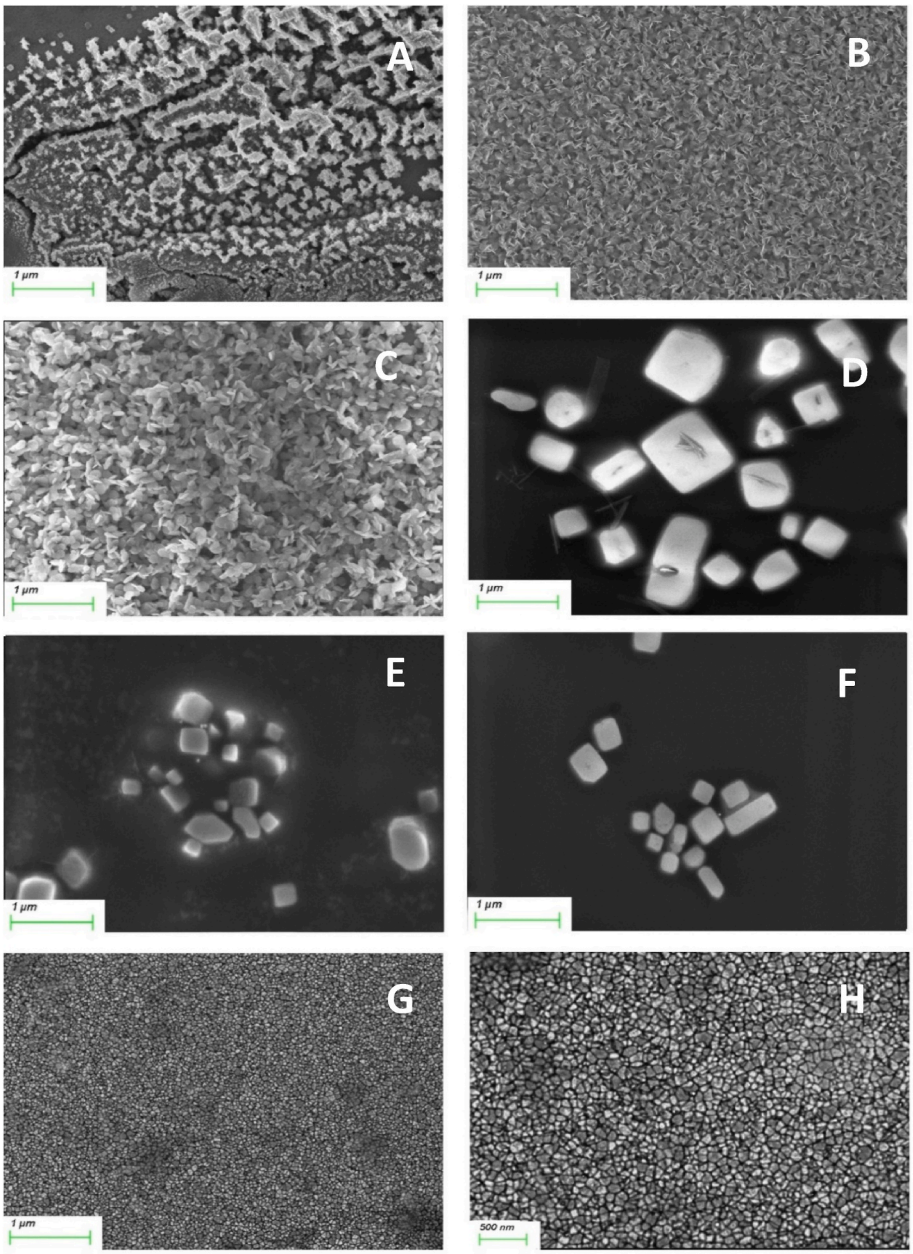

Fig. 1. FE-SEM images of: (A) Cu/ITO, (B) Zn/ITO, (C) Zn/Cu/ITO, (D) BTC/ITO, (E) Cu-BTC/ITO, (F) Zn-BTC/ITO, and (G, H) Zn/Cu-BTC/ITO samples in two different magnifications.

work, in which the smallest particle size of Zn/Cu-BTC/ITO material is clearly discerned.

EDS analysis was performed to reveal the bulk composition of elements in the catalysts (Table 1). Interestingly, the amount of both metals is roughly the same at monometallic MOF catalysts, but a higher insertion of Cu in comparison to Zn was perceived at the bimetallic compound. The last may be attributed to a stronger adhesion of Zn on the surface. This finding was significant, as modifying only specific sites with Zn facilitates the formation of well-defined MOFs, which not only enhance conductivity but also introduce specific active sites. The use of different metals allowed for precise control over the surface structure and properties of the MOF thin films, encompassing aspects such as crystallinity, morphology, roughness and thickness [40].

Table 1
Elemental analysis.

Composition (wt. %)	Zn	Cu	C
BTC/ITO	0	0	100
Zn/ITO	100	0	0
Cu/ITO	0	100	0
Zn-BTC/ITO	70	0	30
Cu-BTC/ITO	0	60	40
Zn/Cu-BTC/ITO	10	70	20

Elemental mapping (Fig. S2) showed a uniform distribution of metal elements on the surface of ITO for the three analyzed Metal/BTC/ITO catalysts. The electrolyte precursors used to form the BTC/ITO composite contain sodium and chloride ions from tributylmethylammonium chloride and sodium methyl sulfate, which are essential for the formation of tributylmethylammonium methyl sulfate (TMS), a key component in the synthesis process. The presence of these elements was confirmed by EDX and is shown in the elemental mapping (Fig. S2).

XRD analysis was conducted to investigate the crystal structure of the materials and to assess the incorporation of Cu and Zn into the microporous BTC structure, as shown in Fig. 2. XRD patterns of Cu-BTC/ITO

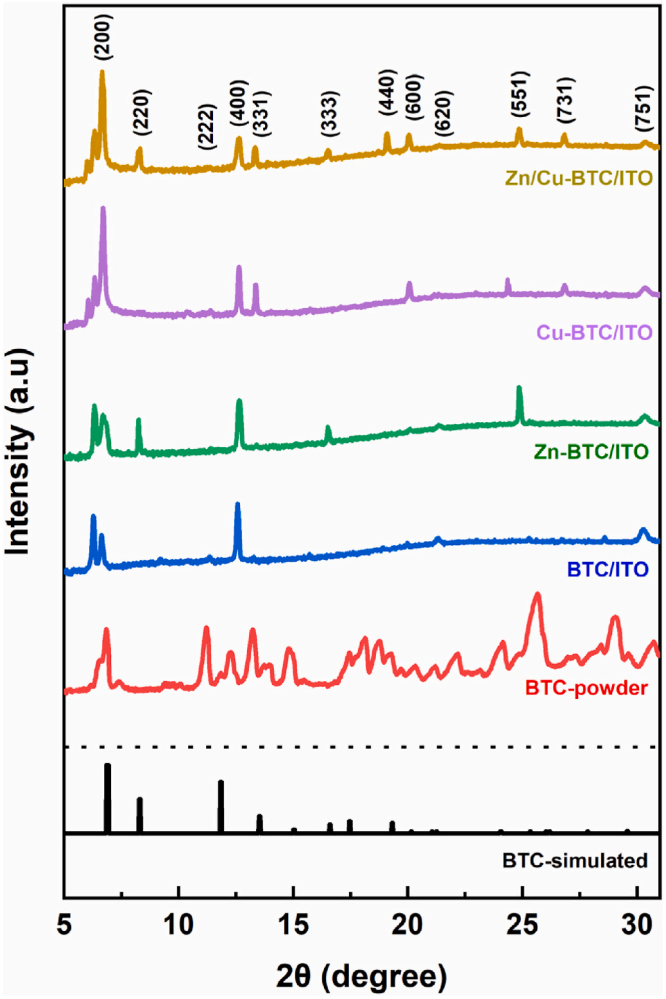

Fig. 2. XRD patterns of BTC-powder (red line), BTC/ITO (blue line), Zn-BTC/ITO (green line), Cu-BTC/ITO (purple line), Zn/Cu-BTC/ITO (yellow line) samples, and BTC-simulated, the crystal data for standard HKUST-1 is stored in the Cambridge Structural Database, deposit number 112954. (For interpretation of the references to colour in this figure legend, the reader is referred to the Web version of this article.)

and Zn-BTC/ITO were found to be consistent with previously reported studies [40–44], confirming that the electrosynthesis of metallic BTC with good crystallinity was successful. These findings further demonstrate the controlled growth of the structures and the formation of a pure phase of the BTC ligand at room temperature in a water-ethanol solution, with a constant voltage applied to the ITO surface.

All electrosynthesized BTC ligand materials exhibited a crystalline structure. Notably, the electrochemical growth process truncated some of the crystalline facets, which were identified as the (220), (331), (333), (440), (600), and (731) crystal planes [40,41,45]. In the case of Zn-BTC/ITO growth, additional crystalline facets were observed, specifically the (220) and (333) planes. Similarly, during the electrochemical growth of Cu-BTC/ITO, new crystalline planes associated with the MOF were identified, including the (331), (440), and (731) planes. When the MOF is modified uniformly and homogeneously, growth occurs in all directions of the material's crystalline planes, as seen in Fig. 3. This agrees with the FE-SEM findings, which revealed that the MOF structures grew in the form of octahedra and tetrahedral (Fig. 1). These results confirm the growth and formation of a pure phase of the Zn/Cu-BTC/ITO structure [40].

Crystallite size of Zn-BTC, Cu-BTC, and Zn/Cu-BTC was calculated according to equation (3) and presented in Table 2. The crystallite size of

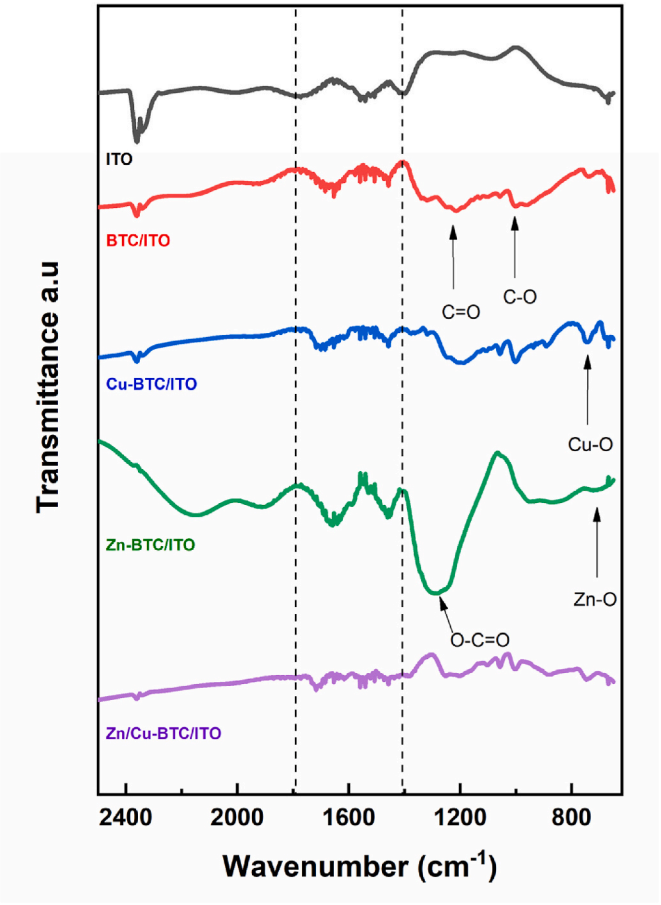

Fig. 3. FTIRS-ATR spectra of ITO (black line), BTC/ITO (red line), Cu-BTC/ITO (blue line), Zn-BTC/ITO (green line), and Zn/Cu-BTC/ITO (purple line) samples. (For interpretation of the references to colour in this figure legend, the reader is referred to the Web version of this article.)

Table 2
X-ray diffraction parameters of Zn/Cu-BTC/ITO, Zn-BTC/ITO and Cu-BTC/ITO samples.

Sample	peak position	FWHM (°)	D (nm)
Zn/Cu-BTC/ITO			
Plane (200)	6.67	0.11	77.36
Plane (220)	8.27	0.12	67.32
Plane (400)	12.67	0.05	156.66
Plane (331)	13.34	159.29	0.053
Plane (333)	16.52	0,13	66.10
Plane (440)	19.09	0.11	79.13
Plane (600)	19.95	1.15	7.35
Plane (551)	24.62	0.09	99.61
Plane (731)	26.84	11.50	0.74
Zn-BTC/ITO			
Plane (200)	6.71	0.07	121.79
Plane (222)	11.62	15.15	0.55
Plane (400)	12.65	0.13	62.68
Plane (333)	16.51	0.06	132.10
Plane (551)	24.87	0.11	80.73
Cu-BTC/ITO			
Plane (200)	6.64	0.24	34.88
Plane (400)	12.64	0.09	90.14
Plane (331)	13.39	0.11	77.41
Plane (600)	20.08	0.13	64.49
Plane (551)	24.33	0.03	334.17
Plane (731)	26.84	0.09	92.19

a MOF can be influenced by the presence of metals in its structure. For instance, when the BTC/ITO is formed without metal, as in the case of the BTC ligand, the interactions are predominantly covalent and hydrogen bonds between the carbon and oxygen atoms of the ligand. These interactions can result in a more compact and uniform structure, leading to a smaller crystallite size [46,47]. The incorporation of a metal (Cu or Zn) in a MOF structure can affect the formation of the molecular framework in several ways. Metals can form coordinated bonds with the ligand, which may lead to an expansion of the structural network. This can result in an increase in crystallite size, as the network becomes less uniform and more susceptible to the aggregation of larger crystallites [48,49]. Additionally, the metal-ligand interactions can impact on the nucleation and growth of crystals, promoting faster growth and, therefore, larger crystallite sizes compared to BTC/ITO without metal [49].

On the other hand, in Zn/Cu-BTC/ITO, which contained two metals in its structure, the metals can compete to bind to the same BTC ligand. This competition could accelerate the nucleation process that results in smaller crystals because the interactions between the metals and the ligands are less predictable and more varied [49,50]. Furthermore, the differences of both metals (i.e. size and shape) can introduce challenges in the assembly of the ligand framework. This can hinder crystal growth, as the steric effects from the metals and the ligand can interfere with the formation of an efficient and compact three-dimensional network [51].

The crystallite size of Zn/Cu-BTC/ITO (Table 2), which was smaller compared to the other MOFs studied, offers distinct advantages in electrocatalysis for HER. Smaller crystallites may induce smaller particles (as was observed in Fig. 1) and consequently an increase of the active surface area, which may facilitate the diffusion of reactants, improve charge transfer, enhance stability, and optimize interactions between the metals and the ligand. These factors may explain why Zn/Cu-BTC/ITO exhibits enhanced catalytic performance for the HER compared to other catalysts, as we are going to discuss in the 3.2 section.

The molecular structure of the MOF is shown in Fig. 3, which reveals a significant absorption band at 740 cm^{-1}, corresponding to the bending and stretching vibrational modes of Cu–O [52]. Additionally, a band near 700 cm^{-1} is attributed to Zn–O interactions [53].

Additionally, bands were identified in the range of 1220–1400 cm^{-1}, which are related to the vibrational modes of C-O bonds and may be associated with carboxyl functional groups (-COOH). It is important to note that the position of these bands can vary depending on the coordination of the metal and its interaction with the BTC ligand [54].

Absorption bands within the range of 900–1150 cm^{-1} are associated with both symmetric and asymmetric vibrational modes of the C=O and C–O stretching vibrations of various functional groups present in the structure. In the shaded region of the spectrum, absorption bands between 1400 and 1800 cm^{-1} can be assigned to the vibrational modes of the carboxylate groups of BTC. These bands are consistent with the asymmetric and symmetric stretching modes of C=O and C–O, respectively, which arise from the coordination of carboxylate (COOH) groups with metal ions. Notably, the peak observed between 1600 and 1700 cm^{-1} confirms the presence of BTC in the catalyst, indicating the successful formation of the metal-BTC structure [52,55].

Photoelectron spectroscopy analysis (XPS) was used to obtain further information on the catalysts surface including the oxidation state of the elements. This information must be interpreted considering its limitations since the catalysts oxidation state probably changes during the electrochemical process.

Fig. 4 shows the Zn 2p (left panel) and Cu 2p (right panel) of Zn/Cu-BTC/ITO catalyst. The lowest intense Zn 2p3/2 component at lower binding energy is attributed to metallic Zn (1021.1 eV, as Zn^0 and/or CuZn alloys), and the component with the highest intensity is associated with Zn^{+2} (1022.7 eV, as ZnO). On the other hand, four Cu satellites signals that are not going to be discussed in the current work are observed. In addition, four signals related to Cu species are observed at more negative values than 940 eV. These species are related to Cu^0 (932.5 eV, as Cu^0 and/or CuZn alloys), Cu^{+1} (933.0 eV, as Cu_2O), Cu^{+2}

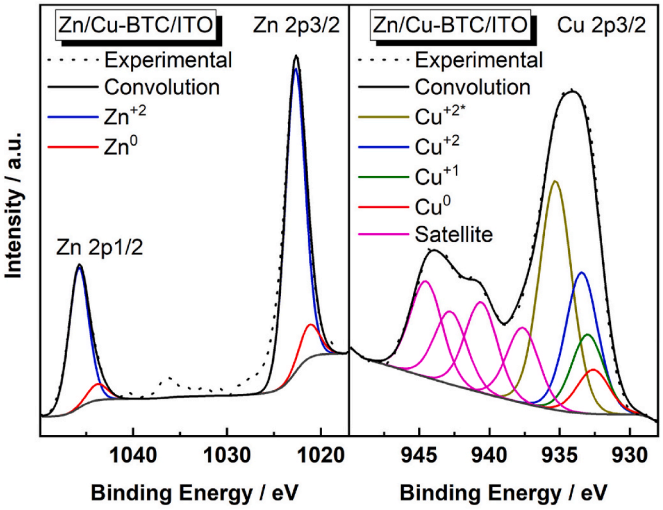

Fig. 4. Zn 2p (left panel) and Cu 2p (right panel) XPS spectra of Zn/Cu-BTC MOF catalyst. Cu^{2+*} refers to $CuOH_2$.

(933.5 eV, as CuO) and Cu^{+2} (935.0 eV, as $Cu(OH)_2$) [44,45,56,57]. These results confirm the formation of the Zn/Cu-BTC MOF and provide a more detailed understanding of its chemical structure and properties. Interestingly, the amount of Cu and Zn detected at the surface of Zn/Cu-BTC/ITO is similar (relative concentration of Cu:Zn ~ 60:40), which contrast with what was observed by EDS. This is due to the fact that XPS and EDS are surface and bulk techniques, respectively. Furthermore, an electronic charge transfer from Zn to Cu seems to happen at Zn/Cu-BTC/ITO material, which may impact the catalytic performance of Zn/Cu-BTC MOF catalyst toward the HER.

3.2. Electrocatalytic studies of modified electrodes

3.2.1. Cyclic voltammetry (CV) study

Studies were conducted to determine the values of electroactive surface areas (ECSA, see 2.3.1 section for experimental description) for various systems using CV at different scan rates and the following values were obtained: Cu/ITO: 0.45 cm^2; Zn/ITO: 0.10 cm^2; Zn/Cu/ITO: 0.53 cm^2; BTC/ITO: 0.20 cm^2; Zn-BTC/ITO: 0.29 cm^2; Cu-BTC/ITO: 0.59 cm^2; Zn/Cu-BTC/ITO: 1.84 cm^2 and 0.77 cm^2 for Pt/ITO (Fig. S3). These results demonstrate the influence of the combination of metals and ligands on the ECSA.

CVs of ITO and BTC/ITO depict very small capacitive and faradaic currents in the potential range under study (Fig. 5). On the other hand, all metal-based electrodes reveal a main anodic peak associated with an oxidation process. For instance, Cu/ITO, Zn/ITO and Zn/Cu/ITO show anodic peaks at 0.39, 0.21 and 0.24 V, respectively. On the other hand, the same redox processes of metal-BTC systems occur at less positive potentials compared to the individual metals, i.e. Cu-BTC/ITO, Zn-BTC/ITO and Zn/Cu-BTC/ITO reveal an anodic peak at 0.23, 0.17 and 0.12 V, respectively. The presence of this anodic peak regardless of the nature of the metal suggests that the catalyst support is oxidizing, which is promoted by the presence of metals onto the ITO surface. The latter effect is even more evident in the presence of BTC and metal species.

On the other hand, Zn/ITO and Zn-BTC/ITO electrodes do not reveal another anodic process, while Cu/ITO and Cu-BTC/ITO materials show an oxidation process at more positive potentials than 0.6 V in the potential range under study. Conversely, the reduction reaction of surface metal oxide species at Cu/ITO, Zn/ITO, Zn/Cu/ITO, Cu-BTC/ITO and Zn-BTC/ITO occurs at similar potential values to the HER, and therefore a cathodic current that involves both processes is discerned. Interestingly, Zn/Cu-BTC/ITO catalyst does not show the anodic peak associated to the catalyst support that is associated to an improved metal

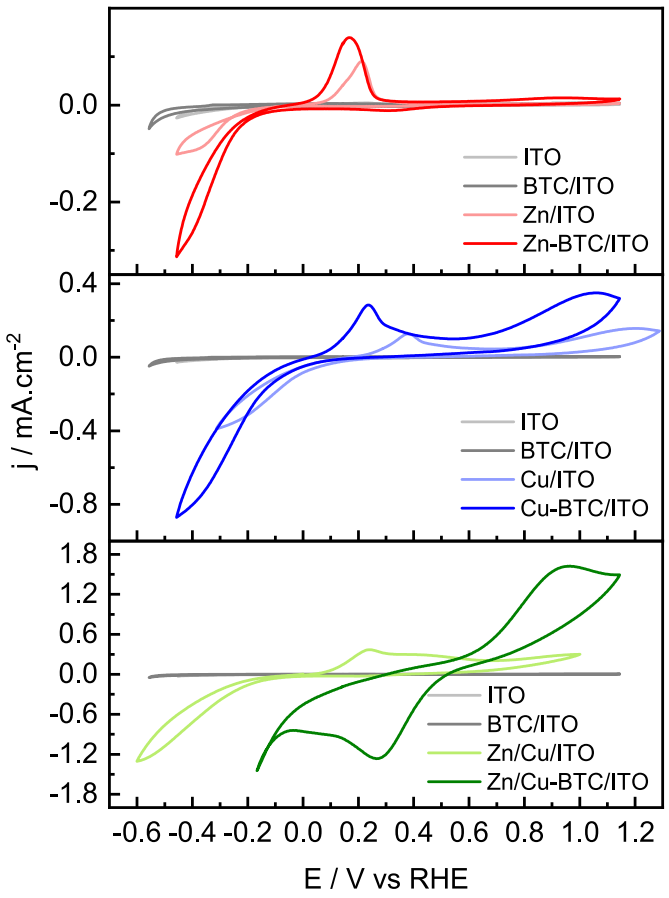

Fig. 5. Cyclic voltammogram recorded at 0.100 V s^{-1} in 0.5 M H_2SO_4 for (top panel) ITO, BTC/ITO, Zn/ITO and Zn-BTC/ITO; (middle panel) ITO, BTC/ITO, Cu/ITO and Cu-BTC/ITO; (bottom panel) ITO, BTC/ITO, Zn/Cu/ITO and Zn/Cu-BTC/ITO.

coverage (see Fig. 1), and reveals quasi-reversible peaks at ca. 0.9 and 0.3 V followed by a cathodic current associated to the HER at potentials more negative than 0.0 V.

In this sense, it is important to emphasize the increase in cathodic current at potentials below 0.0 V in catalysts containing BTC. In particular, the Zn/Cu-BTC/ITO stands out, as it is the only catalyst that shows a cathodic peak around 0.3 V and a notable increase in cathodic current at E < 0.0 V. For example, at −0.2 V, current values of −0.19 mA cm^{-2} were recorded for Cu-BTC/ITO, −0.27 mA cm^{-2} for Zn-BTC/ITO, and −1.10 mA cm^{-2} for Zn/Cu-BTC/ITO. These results highlight the effectiveness of the latter compared to the others.

During the electrochemical tests, no evidence of dissolution due to oxidation was found for Zn/Cu-BTC/ITO electrode during the tests conducted. This suggests that, under the evaluated experimental conditions, the material maintained its structural integrity and no significant losses of zinc or copper in the form of ions were observed. This stability is favorable for the effectiveness of the electrodes in the HER and could indicate good long-term performance in other applications. In addition to the stability observed, the significant improvement in the catalytic performance of the Zn/Cu-BTC/ITO system is not only due to the ECSA surface area, but also to several additional factors. These include the composition and structure of the material, the interaction between the components, and the stability of the system, which optimizes the reaction mechanisms, enhances electron transfer, and reduces energy activation. Furthermore, the synergy generated between Zn and Cu can lead to beneficial effects, while experimental conditions, such as pH and temperature, also play a crucial role in the observed performance.

3.2.2. Reaction mechanism study

To assess the electrocatalytic activity toward the hydrogen evolution reaction (HER) at all materials employed in the current work, linear sweep voltammetry (LSV) experiments were performed in 0.5 M H_2SO_4 solution at 5 mVs^{-1}, as shown in Fig. 6. For comparison, the Pt electrodeposited onto ITO was performed (Pt/ITO). As expected, Pt has a high intrinsic electroactivity, generating a high current density (*j*) with a very low overpotential (η), and an ECSA of 0.77 cm^2.

The unmodified ITO and BTC/ITO electrodes showed no electrocatalytic activity for the HER in the potential range under study. Zn/ITO, Cu/ITO and Zn/Cu/ITO electrodes exhibit poor electrocatalytic activity for the HER. When performing the electrocatalytic study for Zn-BTC/ITO and Cu-BTC/ITO electrodes, they showed a slight improvement in the electrocatalytic performance. In contrast, the catalytic activity was drastically improved with Zn/Cu-BTC/ITO catalyst exhibiting an onset potential close to 0 V, which is quite similar to that of Pt/ITO.

Tafel slope (TS) is a key indicator for studying the kinetics and mechanism of HER. To investigate the reaction mechanism and the rate-determining step (RDS) of the HER at each electrode, Tafel plots were generated from the polarization curves shown in Fig. 6. The linear region of the Tafel plot follows the Tafel equation:

$$(\eta = b \log|j| + a)$$

where $\boldsymbol{\eta}$ is the overpotential, $\boldsymbol{j}$ is the current density, $\boldsymbol{b}$ is the Tafel slope, and $\boldsymbol{a}$ is the intercept corresponding to the exchange current density ($\boldsymbol{j_0}$) [58].

The TS helps to determine the pathway governing the reaction mechanism for HER:

$$\text{Volmer}: H_2O + e^- \rightleftharpoons H_{ad} + OH^- \quad (10)$$

$$\text{Heyrovsky}: H_{ad} + H_2O + e^- \rightleftharpoons H_2 + OH^- \quad (11)$$

$$\text{Tafel}: H_{ad} + H_{ad} \rightleftharpoons H_2 \quad (12)$$

The initial step of the reaction is the same for both pathways. If the Tafel slope is 120 mV dec^{-1}, the rate-limiting step (RDS) is the Volmer reaction. For the Heyrovsky and Tafel mechanisms, the corresponding Tafel slopes are 40 and 30 mV dec^{-1}, respectively [3,31].

Fig. 7 shows a Tafel plot for metal-based electrodes, and their TS indicate the following values: Zn/ITO (136 mV dec^{-1}), Cu/ITO (166 mV dec^{-1}), Zn/Cu/ITO (99 mV dec^{-1}), Zn-BTC/ITO (88 mV dec^{-1}), Cu-BTC/ITO (81 mV dec^{-1}), and Zn/Cu-BTC/ITO (67 mV dec^{-1}) and Pt/

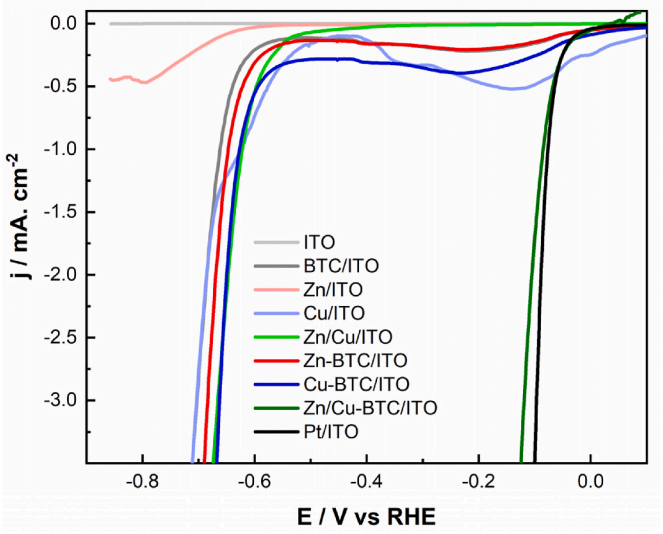

Fig. 6. Linear sweep voltammogram recorded at 0.005 Vs^{-1} in 0.5 M H_2SO_4 solution for all employed catalysts in the current work.

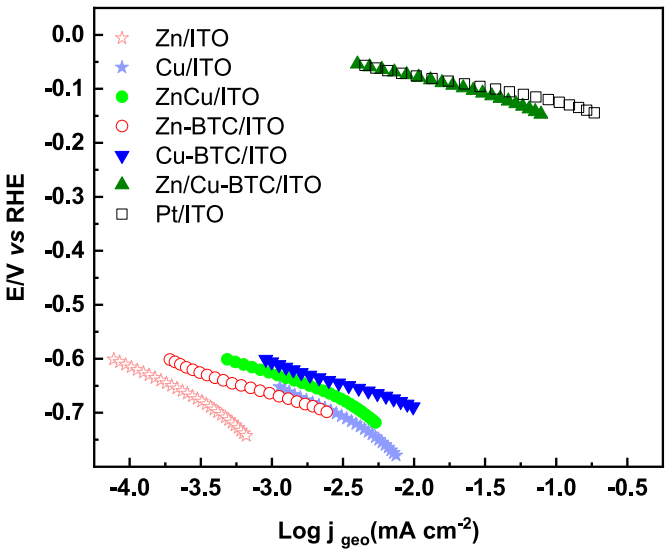

Fig. 7. Tafel plots obtained from Fig. 6 for Zn/ITO, Cu/ITO, Zn/Cu/ITO, Zn-BTC/ITO, Cu-BTC/ITO, Zn/Cu-BTC/ITO and Pt/ITO catalysts.

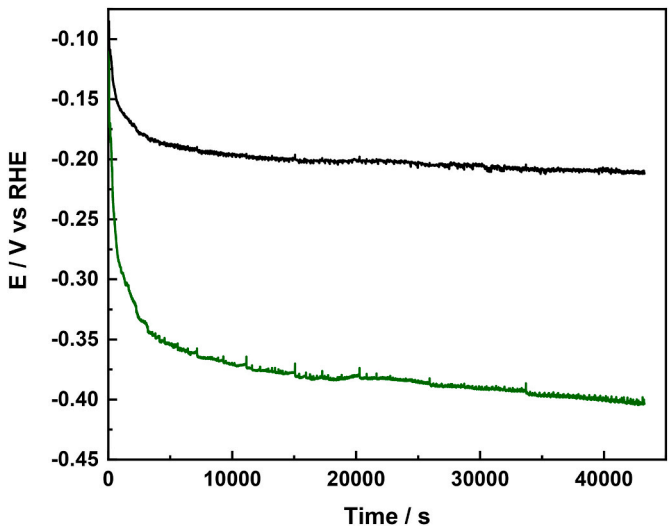

Fig. 8. Potential transient of Zn/Cu-BTC/ITO (green line) and Pt/ITO (black line) recorded at −2 mA/cm^{-2} in 0.5 M H_2SO_4 solution. (For interpretation of the references to colour in this figure legend, the reader is referred to the Web version of this article.)

ITO (52 mV dec^{-1}).

Notably, Pt/ITO catalyst reveals a higher TS value than the expected for bare Pt that is 30 mV dec^{-1} [59,60]. The last suggests another electrochemical reduction reaction in the same potential range in which the HER is occurring, which may be attributed to the electroreduction of surface oxygenated species from the ITO substrate. After that and assuming the described above, it becomes feasible the determination of the RDS at each catalyst. TS values for Zn/ITO, Cu/ITO and Zn/Cu/ITO indicate a similar reaction mechanism with the Volmer step (eq. (10)) as the RDS. On the other hand, the introduction of BTC into the electrode decreases TS values and consequently the RDS appears to be the Heyrovsky step (eq. (11)) for Zn-BTC/ITO, Cu-BTC/ITO and Zn/Cu-BTC/ITO electrodes.

Interestingly, bimetallic electrodes significantly reduce TS at both ITO-based and BTC/ITO-based catalysts, leading to increased exchange current density. Furthermore, bimetallic catalysts in the presence of BTC not only reduce the TS (dark green line in Fig. 7) but also greatly decreases the overpotential to overcome the HER (dark green line in Fig. 6), and consequently the catalytic activity towards the HER is significantly improved.

3.2.3. Catalytic stability and hydrogen quantification study

Electrolysis is an essential electrochemical process for hydrogen production. In this study, electrolysis was performed at a controlled current of −2 mA for more than 12 h. This approach allows for the evaluation of the efficiency and viability of different catalytic systems in hydrogen production.

Fig. 8 shows voltage transients of Zn/Cu-BTC/ITO and Pt/ITO (for comparison since it is the benchmark catalyst) recorded at −2 mA/cm^{-2} in 0.5 M H_2SO_4 solution. The electrochemical performance toward the HER of Zn/Cu-BTC/ITO reveals an overpotential of 0.2 V in comparison to Pt/ITO, which is appropriate taking in account the absence of noble metals, and sustained stability over time. This stable performance over time indicated the electrode's robustness and its ability to withstand prolonged operation without significant degradation.

In order to quantify the Faradaic efficiency (FE) toward the HER, a gas chromatograph (GC) equipped with a micro-volume μTCD detector was employed. Thus, the two most promising catalytic systems were employed: Zn/Cu-BTC/ITO and Pt/ITO. For the Zn/Cu-BTC/ITO electrode system, a hydrogen concentration of 0.159 mM and Faradaic efficiency (FE) of 89.4 % were obtained. In contrast, the Pt/ITO system achieved a hydrogen concentration of 0.169 mM with an FE of 95.1 %. These values are reasonable considering possible losses, gas diffusion out of the system, and imperfections in the material deposition on ITO.

3.2.4. Electrochemical impedance spectroscopy study

The Nyquist diagram obtained from electrochemical impedance spectroscopy (EIS), Fig. 9, allows the evaluation of the charge transfer resistance (Rct) and the efficiency of the different electrodes at the electrode-electrolyte interface. In this case, four systems are compared: Pt/ITO, Cu-BTC/ITO, Zn-BTC/ITO, and Zn/Cu-BTC/ITO. It is observed that Cu-BTC/ITO (blue curve) exhibits the largest arc, indicating a higher charge transfer resistance and, therefore, slower reaction kinetics, probably due to a lower density of catalytically active sites or worse electronic conductivity. In contrast, Zn-BTC/ITO (red curve) and Zn/Cu-BTC/ITO (green curve) present smaller arcs, suggesting a reduction in Rct and an improved charge transport capacity, which is key to optimizing electrocatalytic activity. Pt/ITO (black curve), used as a reference, shows similar impedance than those observed for Zn/Cu-BTC/ITO, confirming the high conductivity and electron transfer of the non-noble metal catalyst [61].

Furthermore, the lower impedance observed for Zn/Cu-BTC/ITO compared to Cu-BTC/ITO implies that the incorporation of Zn into the MOF substantially improves the kinetics of the HER process. This improvement can be attributed to multiple factors, including greater accessibility of the active sites, better dispersion of Zn and Cu in the BTC matrix, and a possible synergy between both metals that favors the adsorption and generation of H_2. Additionally, the lower Rct suggests a more efficient electrode-electrolyte interface, which could be related to an optimization of the material's electronic conductivity or modifications in the hydrogen adsorption energy.

For a more quantitative analysis, the equivalent circuit is shown in Table 3.

In summary, the exceptional catalytic performance of the non-precious metal Zn/Cu-BTC/ITO catalyst toward HER in an acidic medium is due to several factors. The Zn/Cu-BTC material is easily electrosynthesized, providing a simple method for catalyst preparation. This approach offers several advantages, including reduced costs, simpler processing conditions, and the possibility of large-scale production. The Zn/Cu-BTC/ITO material stands out as an excellent catalyst for HER compared to Pt/ITO. Its synergistic effect between the Zn and Cu metals, coupled with a large electrochemically active surface area (ECSA), enables higher reaction efficiency. The morphological features observed in

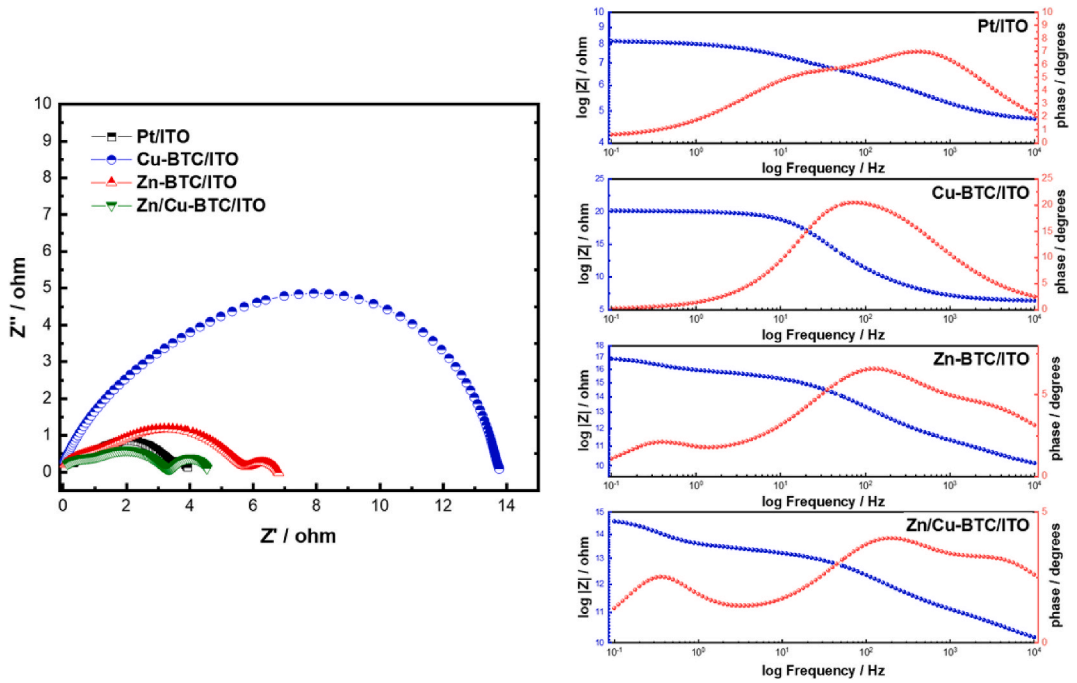

Fig. 9. (Left panel) Nyquist plot (right panel) Bode phase plot for HER at the surface of Pt/ITO, Cu-BTC/ITO, Zn-BTC/ITO, Zn/Cu-BTC/ITO in 0.5 M H_2SO_4.

Table 3
Values obtained from the equivalent circuit for the HER Nyquist diagrams on the surface of Zn-BTC/ITO, Cu-BTC/ITO, Zn/Cu-BTC/ITO and Pt/ITO.

Electrode	Rs (Ω)	Rct1(Ω)	CPE (S^n/Ω)	n	Cdl (μF)	τ (ms)	Equivalent Cirquit
Zn-BTC/ITO	10.21	0.44	5.76×10^{-5}	1.07	2.06	7.00	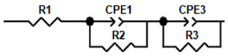
Cu-BTC/ITO	6.23	7.99	3.41×10^{-1}	0.71	2.12×10^{-3}	407	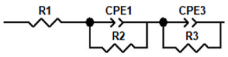
Zn/Cu-BTC/ITO	10.22	2.04	3.62×10^{-1}	0.70	1.67	0.700	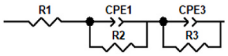
Pt/ITO	4.80	3.13	3.41×10^{-3}	0.70	763	2.39	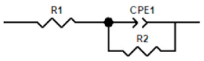

the FE-SEM images, such as reduced particle size and uniform distribution, promote optimal packing in the ITO surface. These combined properties make the Zn/Cu-BTC/ITO catalyst superior in electrochemical applications. Indeed, these attributes make the Zn/Cu-BTC/ITO catalyst a promising catalyst, contributing to the development of more efficient and long-lasting solutions for hydrogen production.

4. Conclusions

This study demonstrates that Zn/Cu-BTC MOFs, prepared via electrodeposition on an ITO surface, exhibit exceptional catalytic performance in the HER. Physicochemical analysis confirms that the uniform dispersion of metals on the ITO surface not only enhances the electrocatalytic activity but also contributes significantly to the long-term stability of the Zn/Cu-BTC/ITO electrode. A key finding is that the morphology of the BTC ligand precursors plays a crucial role in exposing active sites, leading to an increase in the effective surface area of the catalyst. Furthermore, the combination of copper and zinc, along with the high porosity and roughness of Zn/Cu-BTC/ITO, facilitates a shift in the reaction mechanisms, further optimizing the overall catalytic performance. Notably, despite the absence of noble metals, the catalytic performance of Zn/Cu-BTC/ITO is comparable to that of platinum-based catalysts, indicating its great potential for use in renewable energy technologies. These results highlight the importance of continued research to further optimize these materials, ultimately advancing the development of more efficient and cost-effective electrocatalysts for sustainable energy applications.

CRediT authorship contribution statement

Carmen Castro-Castillo: Writing – review & editing, Writing – original draft, Visualization, Resources, Methodology, Investigation, Funding acquisition, Formal analysis, Data curation, Conceptualization. **Rodrigo Espinoza-González:** Supervision, Resources, Funding acquisition, Formal analysis, Conceptualization. **Pedro P. Jofré-Ulloa:** Investigation. **Maximina Luis-Sunga:** Writing – review & editing, Validation, Data curation. **Nataly Silva:** Investigation, Funding acquisition. **Jonathan Suazo-Hernández:** Investigation. **Mónica Soler:** Investigation, Funding acquisition. **Mauricio Isaacs:** Resources. **Gonzalo García:** Writing – review & editing, Validation, Supervision, Funding acquisition, Formal analysis, Conceptualization.

Declaration of competing interest

The authors declare that they have no known competing financial interests or personal relationships that could have appeared to influence the work reported in this paper.

Acknowledgements

C.C-C. thanks the Fondecyt Postdoctoral Grant 3240375, while R.E-G. acknowledges FONDECYT 1231474. C.C-C., R.E-G., and M.S. express their gratitude for Project Anillo FunSeD ACT210059. M.L.-S. acknowledges the doctoral scholarship (TESIS2022010090). Additionally, G.G. thanks MCIN for funding under project PID2020-117586RB-I00 (MCIN/AEI/10.13039/501100011033), as well as NANOtec, INTech, Cabildo de Tenerife, and ULL for providing laboratory facilities. N.S. acknowledges FONDECYT 11221232, P.P.J-U. acknowledges the doctoral fellowship 21221294, and M.I. thanks the Millennium Institute on Green Ammonia as Energy Vector ICN2021_023 (MIGA). The authors also acknowledge the contribution of the MAINI®-UCN Scientific Equipment Unit for providing access to XPS equipment, funded by ANID-FONDEQUIP EQM140044.

Appendix A. Supplementary data

Supplementary data to this article can be found online at https://doi.org/10.1016/j.jpowsour.2025.237480.

Data availability

Data will be made available on request.

References

[1] M.A. Tekalgne, H.H. Do, A. Hasani, Q. Van Le, H.W. Jang, S.H. Ahn, S.Y. Kim, Two-dimensional materials and metal-organic frameworks for the CO2 reduction reaction, Mater. Today Adv. 5 (2020), https://doi.org/10.1016/j.mtadv.2019.100038.

[2] A. Hasani, M.A. Teklagne, H.H. Do, S.H. Hong, Q. Van Le, S.H. Ahn, S.Y. Kim, Graphene-based catalysts for electrochemical carbon dioxide reduction, Carbon Energy 2 (2020) 158–175, https://doi.org/10.1002/cey2.41.

[3] H.H. Do, T.H.C. Nguyen, T. Van Nguyen, C. Xia, D.L.T. Nguyen, P. Raizada, P. Singh, V.H. Nguyen, S.H. Ahn, S.Y. Kim, Q. Van Le, Metal-organic-framework based catalyst for hydrogen production: progress and perspectives, Int. J. Hydrogen Energy 47 (2022) 37552–37568, https://doi.org/10.1016/j.ijhydene.2022.01.080.

[4] M. Luis-Sunga, L. Regent, E. Pastor, G. García, Non-Precious metal graphene-based catalysts for hydrogen evolution reaction, Electrochem 1 (2020), https://doi.org/10.3390/electrochem1020008.

[5] J. Zhu, L. Hu, P. Zhao, L.Y.S. Lee, K.Y. Wong, Recent advances in electrocatalytic hydrogen evolution using nanoparticles, Chem. Rev. 120 (2020) 851–918, https://doi.org/10.1021/acs.chemrev.9b00248.

[6] Y. Zheng, Y. Jiao, A. Vasileff, S.Z. Qiao, The hydrogen evolution reaction in alkaline solution: from theory, single crystal models, to practical electrocatalysts, Angew. Chem. Int. Ed. 57 (2018) 7568–7579, https://doi.org/10.1002/anie.201710556.

[7] A.J. Bard, L.R. Faulkner, in: Electrochemical Methods: Fundamentals and Applications, second ed., JOHN WILEY & SONS, INC., New York, 2001.

[8] M. Zeng, Y. Li, Recent advances in heterogeneous electrocatalysts for the hydrogen evolution reaction, J. Mater. Chem. A Mater. 3 (2015) 14942–14962, https://doi.org/10.1039/c5ta02974k.

[9] J. Kim, J. Oh, S. Baskaran, T.G. Kim, S. Kim, J. Yang, J. Jung, S.M. Yoon, Rhenium redefined as electrocatalyst: hydrogen evolution efficiency boost via Pt and Ni doping, Appl. Catal., B 347 (2024), https://doi.org/10.1016/j.apcatb.2024.123791.

[10] O. Savadogo, P. Montréal, Water electrolysis in acid medium, n.d. https://www.researchgate.net/publication/277045672.

[11] H. Sun, X. Xu, H. Kim, Z. Shao, W.C. Jung, Advanced electrocatalysts with unusual active sites for electrochemical water splitting, InfoMat 6 (2024), https://doi.org/10.1002/inf2.12494.

[12] L.Y. Chang, A.S. Barnard, L.C. Gontard, R.E. Dunin-Borkowski, Resolving the structure of active sites on platinum catalytic nanoparticles, Nano Lett. 10 (2010) 3073–3076, https://doi.org/10.1021/nl101642f.

[13] M.M.E. Duarte, A.S. Pilla, J.M. Sieben, C.E. Mayer, Platinum particles electrodeposition on carbon substrates, Electrochem. Commun. 8 (2006) 159–164, https://doi.org/10.1016/j.elecom.2005.11.003.

[14] M. Bai, T. Ai, W. Bao, J. Han, J. Zhang, Q. Yu, J. Liu, X. Wei, X. Zou, L. Feng, Modulating electronic structure of nickel diselenide by vanadium doping toward highly efficient and stable bifunctional electrocatalysts for overall water splitting, J. Mater. Sci. Technol. 187 (2024) 63–71, https://doi.org/10.1016/j.jmst.2023.11.041.

[15] F. Abdelghafar, X. Xu, S.P. Jiang, Z. Shao, Designing single-atom catalysts toward improved alkaline hydrogen evolution reaction, Mater. Reports: Energy 2 (2022), https://doi.org/10.1016/j.matre.2022.100144.

[16] Y. Luo, Y. Zhang, J. Zhu, X. Tian, G. Liu, Z. Feng, L. Pan, X. Liu, N. Han, R. Tan, Material engineering strategies for efficient hydrogen evolution reaction catalysts, Small Methods (2024), https://doi.org/10.1002/smtd.202400158.

[17] A. Bayaguud, Y. Fu, C. Zhu, Interfacial parasitic reactions of zinc anodes in zinc ion batteries: underestimated corrosion and hydrogen evolution reactions and their suppression strategies, J. Energy Chem. 64 (2022) 246–262, https://doi.org/10.1016/j.jechem.2021.04.016.

[18] J. Zhao, G. Zhang, H. Liu, Q. Shu, Q. Zhang, Improved charge transfer and morphology on Ti-modified Cu/γ-Al2O3/Al catalyst enhance the activity for methanol steam reforming, Int. J. Hydrogen Energy 47 (2022) 18294–18304, https://doi.org/10.1016/j.ijhydene.2022.04.025.

[19] P. Farinazzo Bergamo Dias Martins, P. Papa Lopes, E.A. Ticianelli, V. R. Stamenkovic, N.M. Markovic, D. Strmcnik, Hydrogen evolution reaction on copper: promoting water dissociation by tuning the surface oxophilicity, Electrochem. Commun. 100 (2019) 30–33, https://doi.org/10.1016/j.elecom.2019.01.006.

[20] W. Lu, R. Zhang, S. Toan, R. Xu, F. Zhou, Z. Sun, Z. Sun, Microchannel structure design for hydrogen supply from methanol steam reforming, Chem. Eng. J. 429 (2022), https://doi.org/10.1016/j.cej.2021.132286.

[21] X. Vecino, M. Reig, J. López, C. Valderrama, J.L. Cortina, Valorisation options for Zn and Cu recovery from metal influenced acid mine waters through selective precipitation and ion-exchange processes: promotion of on-site/off-site management options, J. Environ. Manag. 283 (2021), https://doi.org/10.1016/j.jenvman.2021.112004.

[22] G. Barati Darband, M. Aliofkhazraei, S. Hyun, A. Sabour Rouhaghdam, S. Shanmugam, Electrodeposition of Ni-Co-Fe mixed sulfide ultrathin nanosheets on Ni nanocones: a low-cost, durable and high performance catalyst for electrochemical water splitting, Nanoscale 11 (2019) 16621–16634, https://doi.org/10.1039/c9nr04529e.

[23] R.L. Zhang, J.J. Duan, L.P. Mei, J.J. Feng, P.X. Yuan, A.J. Wang, Facile synthesis of porous iridium-palladium-plumbum wire-like nanonetworks with boosted catalytic performance for hydrogen evolution reaction, J. Colloid Interface Sci. 580 (2020) 99–107, https://doi.org/10.1016/j.jcis.2020.06.124.

[24] J. Gao, Q. Huang, Y. Wu, Y.Q. Lan, B. Chen, Metal–organic frameworks for photo/electrocatalysis, Adv. Energy Sustain. Res. 2 (2021), https://doi.org/10.1002/aesr.202100033.

[25] Y. Wu, Y. Li, J. Gao, Q. Zhang, Recent advances in vacancy engineering of metal-organic frameworks and their derivatives for electrocatalysis, SusMat 1 (2021) 66–87, https://doi.org/10.1002/sus2.3.

[26] H. Wang, Q.L. Zhu, R. Zou, Q. Xu, Metal-organic frameworks for energy applications, Chem 2 (2017) 52–80, https://doi.org/10.1016/j.chempr.2016.12.002.

[27] W.J. Li, M. Tu, R. Cao, R.A. Fischer, Metal-organic framework thin films: electrochemical fabrication techniques and corresponding applications & perspectives, J. Mater. Chem. A Mater. 4 (2016) 12356–12369, https://doi.org/10.1039/c6ta02118b.

[28] T. Qiu, Z. Liang, W. Guo, H. Tabassum, S. Gao, R. Zou, Metal–organic framework-based materials for energy conversion and storage, ACS Energy Lett. 5 (2020) 520–532, https://doi.org/10.1021/acsenergylett.9b02625.

[29] B. Zhu, D. Xia, R. Zou, Metal-organic frameworks and their derivatives as bifunctional electrocatalysts, Coord. Chem. Rev. 376 (2018) 430–448, https://doi.org/10.1016/j.ccr.2018.07.020.

[30] F. Sun, Q. Li, H. Xue, H. Pang, Pristine transition-metal-based metal-organic frameworks for electrocatalysis, ChemElectroChem 6 (2019) 1273–1299, https://doi.org/10.1002/celc.201801520.

[31] M. malakzadeh, J.B. Raoof, A. Ghafarnejad, R. Ojani, In-situ electrosynthesis Cu-PtBTC MOF-derived nanocomposite modified glassy carbon electrode for highly performance electrocatalysis of hydrogen evolution reaction, J. Electroanal. Chem. 900 (2021), https://doi.org/10.1016/j.jelechem.2021.115716.

[32] T. Rodenas, I. Luz, G. Prieto, B. Seoane, H. Miro, A. Corma, F. Kapteijn, F.X. Llabrés I Xamena, J. Gascon, Metal-organic framework nanosheets in polymer composite materials for gas separation, Nat. Mater. 14 (2015) 48–55, https://doi.org/10.1038/nmat4113.

[33] S. Hermes, M.K. Schröter, R. Schmid, L. Khodeir, M. Muhler, A. Tissler, R. W. Fischer, R.A. Fischer, Metal@MOF: loading of highly porous coordination polymers host lattices by metal organic chemical vapor deposition, Angew. Chem. Int. Ed. 44 (2005) 6237–6241, https://doi.org/10.1002/anie.200462515.

[34] C.S. Lee, J.M. Lim, J.T. Park, J.H. Kim, Direct growth of highly organized, 2D ultra-thin nano-accordion Ni-MOF@NiS2@C core-shell for high performance energy storage device, Chemical Engineering Journal 406 (2021), https://doi.org/10.1016/j.cej.2020.126810.

[35] H.W. Jee, K.J. Paeng, N. Myung, K. Rajeshwar, Electrochemical deposition of a metal-organic framework and subsequent conversion to cobalt selenide, ACS Appl. Electron. Mater. 2 (2020) 1358–1364, https://doi.org/10.1021/acsaelm.0c00142.

[36] F. Hasani, J.B. Raoof, M. Ghani, R. Ojani, In situ electrodeposition of Cu-BDC metal–organic framework on pencil graphite substrate for solid-phase microextraction of some pesticides, Microchim. Acta 189 (2022), https://doi.org/10.1007/s00604-022-05537-6.

[37] A. Verdaguer-Casadevall, C.W. Li, T.P. Johansson, S.B. Scott, J.T. McKeown, M. Kumar, I.E.L. Stephens, M.W. Kanan, I. Chorkendorff, Probing the active surface

sites for CO reduction on oxide-derived copper electrocatalysts, J. Am. Chem. Soc. 137 (2015) 9808–9811, https://doi.org/10.1021/jacs.5b06227.
[38] D. Gao, J. Guo, X. Cui, L. Yang, Y. Yang, H. He, P. Xiao, Y. Zhang, Three-dimensional dendritic structures of NiCoMo as efficient electrocatalysts for the hydrogen evolution reaction, ACS Appl. Mater. Interfaces 9 (2017) 22420–22431, https://doi.org/10.1021/acsami.7b04009.
[39] N.M. Mahmoodi, J. Abdi, Nanoporous metal-organic framework (MOF-199): Synthesis, characterization and photocatalytic degradation of basic Blue 41, Microchem. J. 144 (2019) 436–442, https://doi.org/10.1016/j.microc.2018.09.033.
[40] M. Liao, H. Qin, W. Guo, P. Gao, J. Liu, H. Xiao, Hydrogen production employing Cu/Zn-BTC metal-organic framework on cordierite honeycomb ceramic support in methanol steam reforming process within a microreactor, Int. J. Hydrogen Energy 47 (2022) 35136–35148, https://doi.org/10.1016/j.ijhydene.2022.08.125.
[41] Y. Mao, L. Shi, H. Huang, W. Cao, J. Li, L. Sun, X. Jin, X. Peng, Room temperature synthesis of free-standing HKUST-1 membranes from copper hydroxide nanostrands for gas separation, Chem. Commun. 49 (2013) 5666–5668, https://doi.org/10.1039/c3cc42601g.
[42] Z. Wang, J. Wang, M. Li, K. Sun, C.J. Liu, Three-dimensional printed acrylonitrile butadiene styrene framework coated with Cu-BTC metal-organic frameworks for the removal of methylene blue, Sci. Rep. 4 (2014), https://doi.org/10.1038/srep05939.
[43] M. Meilikhov, K. Yusenko, E. Schollmeyer, C. Mayer, H.J. Buschmann, R.A. Fischer, Stepwise deposition of metal organic frameworks on flexible synthetic polymer surfaces, Dalton Trans. (2003) 40 (2011) 4838–4841, https://doi.org/10.1039/c0dt01820a.
[44] S. Jabarian, A. Ghaffarinejad, Simultaneous electrosynthesis of Cu-BTC and Zn-BTC metal-organic frameworks on brass, New J. Chem. 44 (2020) 19820–19826, https://doi.org/10.1039/d0nj04303f.
[45] R. Wu, D.P. Wang, V. Kumar, K. Zhou, A.W.K. Law, D. Pooi, S. Lee, J. Lou, Z. Chen, Supporting Information MOFs-Derived Copper Sulfides Embedded Within Porous Carbon Octahedra for Electrochemical Capacitor Applications, 2015.
[46] P. Jutrzenka Trzebiatowska, Z. Maramorosz, M.A. Baluk, M. Gazda, A. Ecieza, A. Zaleska-Medynska, The catalytic activity of metal–organic frameworks (MOFs) and post-synthetic modified MOF towards depolymerisation of polycarbonate, Appl. Surf. Sci. 673 (2024), https://doi.org/10.1016/j.apsusc.2024.160894.
[47] F. Vermoortele, R. Ameloot, L. Alaerts, R. Matthessen, B. Carlier, E.V.R. Fernandez, J. Gascon, F. Kapteijn, D.E. De Vos, Tuning the catalytic performance of metal-organic frameworks in fine chemistry by active site engineering, J. Mater. Chem. 22 (2012) 10313–10321, https://doi.org/10.1039/c2jm16030g.
[48] F. Ahmad, K. Rafiq, T. Najam, E. Hussain, M. Sohail, M.Z. Abid, A. Mahmood, M. S. Javed, S.S.A. Shah, Metal-organic frameworks for electrocatalytic water-splitting: beyond the pyrolysis, Int. J. Hydrogen Energy 48 (2023) 35075–35111, https://doi.org/10.1016/j.ijhydene.2023.05.247.
[49] J. Łuczak, M. Kroczewska, M. Baluk, J. Sowik, P. Mazierski, A. Zaleska-Medynska, Morphology control through the synthesis of metal-organic frameworks, Adv. Colloid Interface Sci. 314 (2023), https://doi.org/10.1016/j.cis.2023.102864.
[50] X. Li, S. Li, J. Liu, J. Zhang, Y. Ren, J. Zhao, Construction of Zn-Cu bimetallic metal-organic frameworks for carbon dioxide capture, RSC Adv. 14 (2024) 20780–20785, https://doi.org/10.1039/d4ra03539a.
[51] A. Heuer-Jungemann, N. Feliu, I. Bakaimi, M. Hamaly, A. Alkilany, I. Chakraborty, A. Masood, M.F. Casula, A. Kostopoulou, E. Oh, K. Susumu, M.H. Stewart, I. L. Medintz, E. Stratakis, W.J. Parak, A.G. Kanaras, The role of ligands in the chemical synthesis and applications of inorganic nanoparticles, Chem. Rev. 119 (2019) 4819–4880, https://doi.org/10.1021/acs.chemrev.8b00733.
[52] R. Nivetha, A. Sajeev, A. Mary Paul, K. Gothandapani, S. Gnanasekar, G. Jacob, R. Sellappan, V. Raghavan, N. Krishna Chandar, S. Pitchaimuthu, S.K. Jeong, A. Nirmala Grace, Cu based metal organic framework (Cu-MOF) for electrocatalytic hydrogen evolution reaction, Mater. Res. Express 7 (2020), https://doi.org/10.1088/2053-1591/abb056.
[53] S. Haider, M. Zaib, U. Farooq, M. Saeed, M. Salman, R.A. Bajwa, Fabrication of zinc oxide and zinc oxide-copper-benzene tricarboxylic acid-modified carbon paste electrodes as electrochemical sensor for Cd (II) ions, Arabian J. Sci. Eng. 48 (2023) 7485–7500, https://doi.org/10.1007/s13369-022-07542-6.
[54] W.W. Lestari, J. Hartono, M. Adreane, K.D. Nugrahaningtyas, C. Purnawan, S. B. Rahardjo, Electro-synthetic optimization of host material based on MIL-100(Fe), Molekul 11 (2016) 61, https://doi.org/10.20884/1.jm.2016.11.1.195.
[55] M.J. Neufeld, J.L. Harding, M.M. Reynolds, Immobilization of metal-organic framework Copper(II) Benzene-1,3,5-tricarboxylate (CuBTC) onto cotton fabric as a nitric oxide release catalyst, ACS Appl. Mater. Interfaces 7 (2015) 26742–26750, https://doi.org/10.1021/acsami.5b08773.
[56] P. Gao, X.Y. Sun, B. Liu, H.T. Lian, X.Q. Liu, J.S. Shen, Cu MOF-based catalytic sensing for formaldehyde, J. Mater. Chem. C Mater. 6 (2018) 8105–8114, https://doi.org/10.1039/c8tc01703d.
[57] T.T. Minh, N.T.T. Tu, T.T. Van Thi, L.T. Hoa, H.T. Long, N.H. Phong, T.L.M. Pham, D.Q. Khieu, Synthesis of porous octahedral ZnO/CuO composites from Zn/Cu-based MOF-199 and their applications in visible-light-driven photocatalytic degradation of dyes, J. Nanomater. 2019 (2019), https://doi.org/10.1155/2019/5198045.
[58] Y.H. Fang, Z.P. Liu, Tafel kinetics of electrocatalytic reactions: from experiment to first-principles, ACS Catal. 4 (2014) 4364–4376, https://doi.org/10.1021/cs501312v.
[59] S. Zhao, A.E. Wangstrom, Y. Liu, W.A. Rigdon, W.E. Mustain, Stability and activity of Pt/ITO electrocatalyst for oxygen reduction reaction in alkaline media, Electrochim. Acta 157 (2015) 175–182, https://doi.org/10.1016/j.electacta.2015.01.030.
[60] V.T.T. Ho, H.Q. Pham, T.H.T. Anh, A. Van Nguyen, K.A.N. Quoc, H.T.H. Vo, T. T. Nguyen, Highly stable Pt/ITO catalyst as a promising electrocatalyst for direct methanol fuel cells, C. R. Chim. 22 (2019) 838–843, https://doi.org/10.1016/j.crci.2019.08.003.
[61] X. Cao, Y. Gao, Y. Li, D.M. Weragoda, G. Tian, W. Zhang, Z. Zhang, X. Zhao, B. Chen, Research progress on MOFs and their derivatives as promising and efficient electrode materials for electrocatalytic hydrogen production from water, RSC Adv. 13 (2023) 24393–24411, https://doi.org/10.1039/d3ra04110g.